

Self-referenced subcycle metrology of quantum fields

Sinan Gündoğdu* Stéphane Virally Marco Scaglia Denis V. Seletskiy* Andrey S. Moskalenko*

Sinan Gundogdu, Andrey S. Moskalenko

Department of Physics, KAIST, Daejeon 34141, Republic of Korea

Email Address: moskalenko@kaist.ac.kr

Sinan Gundogdu

Center for Theoretical Physics of Complex Systems, Institute for Basic Science (IBS), Daejeon 34126, Republic of Korea

Email Address: gu.sinan@gmail.com

Stéphane Virally, Marco Scaglia, Denis V. Seletskiy

femtoQ Lab, Department of Engineering Physics, Polytechnique Montréal, Montréal, QC H3T 1J4, Canada

Email Address: denis.seletskiy@polymtl.ca

Keywords: *Quantum metrology, Electro-optic sampling, Balanced homodyne detection, Ultrabroadband, Quantum vacuum, Cat states*

We propose and analyze a new time-domain method for subcycle metrology of quantum electric fields using a combination of a 3rd order nonlinear optical process and homodyne detection with a local oscillator (LO) field. The new method enables isolation of intrinsically weak quantum noise contribution by subtraction of the shot noise of the LO on a pulse-by-pulse basis. Together with the centro-symmetric character of the nonlinearity, our method unlocks novel opportunities toward terahertz and mid-infrared quantum field metrologies.

1 Introduction

Homodyne detection (HD) [1] is a central technique of signal analysis in quantum optics. A quantum field under study interferes on a photo-diode with a strong classical mode E_{LO} , termed local oscillator (LO) [2]. Fitting for the visible and near-infrared frequency bands, HD of quantum fields in the range from mid-infrared (MIR) to terahertz (THz) is challenged by a general unavailability of bright sources of classical LO and high-efficiency photo-diodes. Despite such challenges, interest in these frequency bands is largely motivated by direct sensing of unique signature absorption features in solid-state, liquid and gaseous targets [3]. Parallel developments in short-pulse lasers [4] and measurement techniques, such as electro-optic sampling (EOS) [5, 6, 7], have stimulated metrology of classical fields at terahertz (THz) to mid-infrared (MIR) frequencies, and above [8, 9, 10, 11, 12, 13]. As an EOS setup, consider a signal E_T at a low center frequency Ω (e.g. THz or MIR) and a probe pulse E_P at a high center frequency ω_0 (e.g. near-infrared, NIR) and bandwidth $\Delta\omega$ that co-propagate inside of a second-order ($\chi^{(2)}$) nonlinear crystal with electro-optic activity. A mixing product of this interaction, $E_T \cdot E_P$, can span over frequencies $\omega_0 \pm \Omega$, in spectral overlap with the probe pulse when $2\Omega < \Delta\omega$. The resulting interference is exploited for the EOS detection of instantaneous amplitude E_T , resolved as a function of time difference τ between E_P and E_T , provided that the bandwidth of the probe field E_P is larger than $2/T$, where T is the characteristic cycle period of the signal field E_T . In contrast to HD and its generalizations to the pulsed LO case [14, 15, 16, 17, 18, 19], EOS is an intrinsically time-domain technique, alleviating the need for direct detection of the signal field.

Recent demonstrations ported EOS to the quantum regime, showing direct sampling of a quantum vacuum field [20, 21], and even measuring the spatio-temporal correlations [22] and causal structure of the electromagnetic ground state [23]. Such developments promise direct routes toward MIR and THz quantum sensing technologies, while the time-domain character motivates new metrology protocols [24, 25, 26] as well as a path toward experimental quantum electrodynamics in space-time [27, 28, 29, 30, 23]. Despite this progress, time domain quantum photonics faces a few outstanding challenges. On the one hand, strong phonon-polariton dispersion in the $\chi^{(2)}$ crystal used in EOS makes the detection of signals around the Reststrahlen band frequencies challenging [6, 7]. On the other, the fractional content of the quantum contribution to the variance of the total detected signal amounts to only a few percent of the shot-noise of E_P [21]. Experimental differentiation between the two contributions must be exquisitely

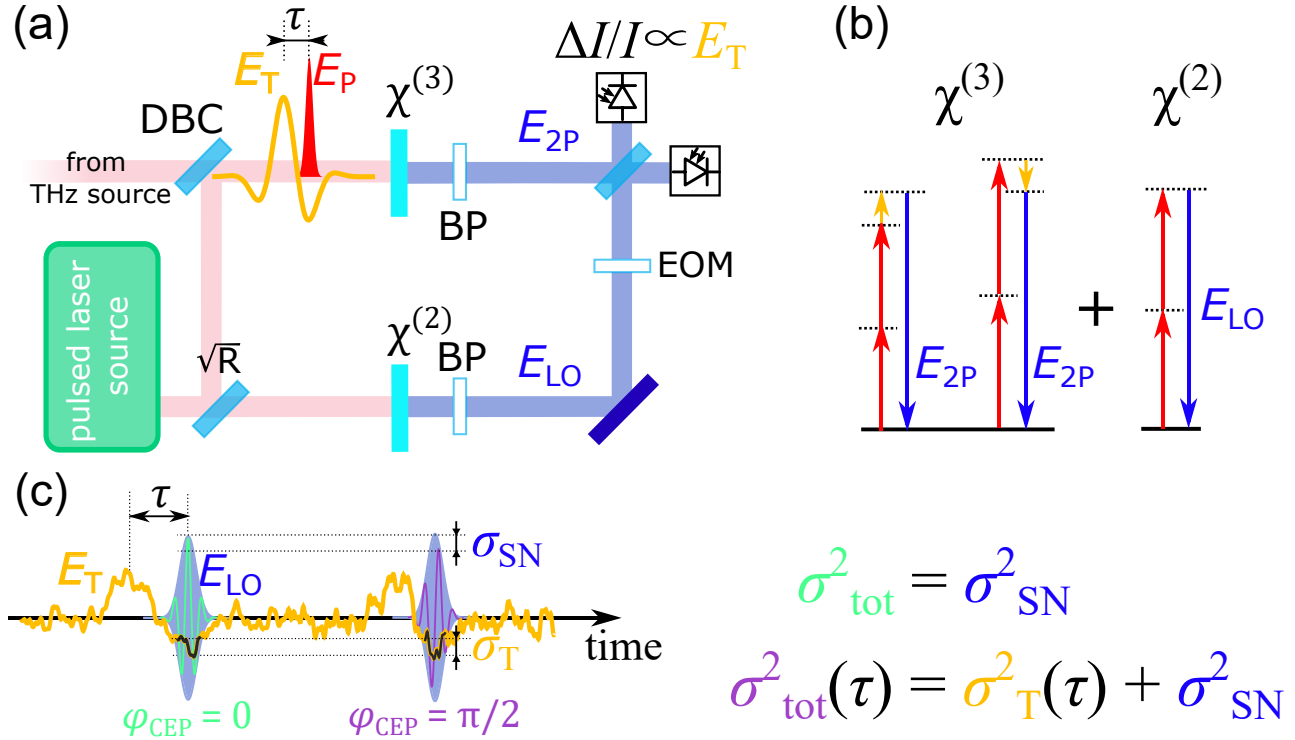


Figure 1: (a) Proposed metrology scheme. The output of a near-infrared (NIR) pulsed laser source is split in two arms. Upper arm: E_T [THz signal (orange)] and a part of E_P [NIR probe (red)] are time-delayed by τ , overlapped via a dichroic beam combiner (DBC), and mixed in a $\chi^{(3)}$ crystal to generate E_{2P} signal (blue). Lower arm: E_{LO} [Local oscillator (LO, blue)] is derived from a frequency-doubled remainder of E_P and passes through an electro-optic modulator (EOM). After bandpass filters (BP), E_{LO} and E_{2P} are mixed in a balanced homodyne detector, schematized as a superposition of $\chi^{(3)}$ and $\chi^{(2)}$ processes in (b). (c) EOM-shifted E_{LO} contains a $\pi/2$ flip of the CEP between consecutive pulses, so that their total noise variance σ_{tot} is oscillating between having only shot-noise contribution σ_{SN} or also containing the variance of the quantum field $\sigma_T(\tau)$.

precise [20], ideally requiring pulse-by-pulse comparison [27] of events with and without the quantum contribution, a feat that is not currently available experimentally.

In this Letter, we propose a new scheme for time-domain metrology of quantum signals based on the third-order ($\chi^{(3)}$) nonlinear interaction between quantum E_T and classical E_P , admitting full access to the term carrying interference of E_{LO} and the signal fields [31, 32, 33]. In the four-wave mixing, the THz-induced second-harmonic (TFISH) signal arises from the nonlinear mixing product $E_P \cdot E_P \cdot E_T$ at frequencies $2\omega_0 \pm \Omega$, which can be superposed in a background-free manner with the E_{LO} centered at $2\omega_0$. We show that this freedom opens an elegant opportunity for a direct self-referenced measurement of the quantum contribution to the signal variance, based on a shot-by-shot carrier-envelope phase (CEP) modulation on E_{LO} of a free-running frequency comb [34]. Furthermore, dipole inactivity of optical phonons in common inversion-symmetric materials positions the $\chi^{(3)}$ -based scheme for efficient field-resolved detection in the 5-15 THz band, which is generally problematic for a host of EOS detection crystals [7]. Finally, the new scheme does not require analysis of the polarization state of the probe, relaxing constraints on broadband polarization optics [25].

2 Generation of the TFISH and LO fields

Figure 1 shows the schematic of the proposed metrology scheme. It consists of an interferometer with two paths. The upper path combines E_T , the THz signal to be characterized, and one part of the NIR probe pulse $E'_P = \sqrt{R}E_P$, both passing through a $\chi^{(3)}$ nonlinear crystal to generate the TFISH signal E_{2P} . In the lower path, the second part of the probe $\sqrt{1-R}E_P$ undergoes a broadband second harmonic generation (SHG) process in a $\chi^{(2)}$ nonlinear crystal, to generate the LO pulse E_{LO} centered at a

frequency $2\omega_0$. E_{2P} is mixed with E_{LO} at a beamsplitter, and analyzed by the balanced homodyne detection technique. The measurement system is based on a free running frequency comb, whereas an external EOM provides an opportunity to control the carrier-envelope phase shift $\Delta\phi_{CEP}$ of the LO field on a pulse-by-pulse basis. This feature is exploited for the self-referenced detection, where the difference in the variance sampled by two adjacent LO pulses isolates the quantum contribution (**Figure 1c**), as detailed below.

The total electric field passing through the $\chi^{(3)}$ crystal, E , can be represented as a sum: $E = E'_P + E_{2P} + E_T$. When E_T corresponds to a quantum signal, its properties together with those of E_{2P} and E , should be described in terms of operators denoted as \hat{E}_T , \hat{E}_{2P} and \hat{E} , respectively. Since the probe is a strong coherent field, it is sufficient here to describe it classically using the corresponding mean value $\langle \hat{E}'_P \rangle \equiv E'_P$. Thus, the generation of \hat{E}_{2P} is described by the third order nonlinear polarization:

$$\hat{P}_{2P}^{NL} = 3\epsilon_0\chi^{(3)}RE_P'^{(+) }E_P'^{(+) }[\hat{E}_T^{(+)} + \hat{E}_T^{(-)}] + \text{H.c.}, \quad (1)$$

where we have decomposed E'_P (\hat{E}_T) into its positive $E_P'^{(+)}$ ($\hat{E}_T^{(+)}$) and negative $E_P'^{(-)}$ ($\hat{E}_T^{(-)}$) frequency parts [35]. ϵ_0 is the vacuum permittivity. We have assumed that the interaction can be well described by an effective $\chi^{(3)}$ constant, neglecting its frequency dependence. Further, we consider such a crystal orientation that it is sufficient to include only one linear polarization component for each of the involved fields. We also ignore any other third order nonlinear polarization terms since they are comparably much weaker, due to the fact that E'_P is a strong coherent field and \hat{E}_T is a weak quantum signal, or the corresponding generated field contributions are removed by an appropriate bandpass filter before the final beamsplitter. Under these general assumptions, we can describe the electromagnetic wave propagation in the $\chi^{(3)}$ crystal using the inhomogeneous wave equation within the slowly varying amplitude approximation (SVAA) for plane waves. We decompose all fields, $X = E'_P, \hat{E}_T, \hat{E}_{2P}, \hat{P}_{NL}$, into forward-propagating plane waves as $X(z, t) = \int_0^\infty X(z, \omega)e^{i[k(\omega)z - \omega t]}d\omega + \text{H.c.}$ using a convention $X(z, \omega) \equiv 0$ for $\omega < 0$, $X^{(+)}(z, \omega) \equiv X(z, \omega)$, and $X^{(-)}(z, -\omega) = [X(z, \omega)^{(+)}]^\dagger$, which has to be taken into account for convolutions we define below. Then solving the propagation equation for the TFISH under the assumptions of small crystal thickness d and negligible depletion of the probe, we obtain (cf. Supporting Information):

$$\hat{E}_{2P}(\omega_2) = idA_P^2C(\omega_2)(\mathcal{R} * (\hat{E}_T^{(+)} + \hat{E}_T^{(-)}))(\omega_2) + \hat{E}_B(\omega_2). \quad (2)$$

Here $*$ denotes convolution and $C(\omega) = 3\chi^{(3)}R\omega/[2cn(\omega)]$, where $n(\omega)$ is the frequency-dependent refractive index and c is the speed of light in vacuum. We decomposed $E_P = A_P f(\omega)$ into its (real) amplitude A_P and (generally complex) normalized frequency distribution $f(\omega)$, defining a gating function $\mathcal{R}(\omega_2) = (f * f)(\omega_2)e^{-i\omega_2\tau}$. The time τ corresponds to the center of the probe pulse relative to the incoming THz field (**Figure 1a**). Finally, $\hat{E}_B(\omega_2)$ is the co-propagating background vacuum field, existing even in the absence of the probe field. As we will see below, this contribution can be directly characterized in the current setup by studying the signal variance when $\phi_{CEP} = 0$ (cf. **Figure 1c**) is induced on the LO field. In the above derivation, we have neglected the back-action effect of the $\chi^{(3)}$ interaction on the co-propagating THz field \hat{E}_T [36]. That is appropriate if the first term on the right-hand side of Equation (2) represents a small correction to the second term and is in accordance with our evaluation of the variance signals.

3 Homodyne detection

As described, homodyne detection is enabled by letting \hat{E}_{2P} interfere with the LO field E_{LO} which is produced via the SHG in the $\chi^{(2)}$ crystal. The SHG process can be realized with a high conversion efficiency η_2 , and the resulting mode $f_{LO}(\omega)$ of the LO still closely resembles the mode of the TFISH field. For the details of a possible realization, see Supporting Information. Since the LO represents a strong coherent field, we can describe it classically for the homodyning part of the setup. At the beamsplitter before the detectors, we can express it in the frequency domain as $E_{LO}(\omega_2) = Ae^{-i\phi}e^{-i\omega_2\tau}f_{LO}(\omega_2)$, where

$A = \sqrt{\eta_2} \sqrt{1 - R} A_P$ is the amplitude and ϕ is a variable CEP induced by the EOM. An elegant alternative realization of such phase shift between the two arms of the setup can be provided by a dual frequency comb [37]. We assume the LO has effectively the same time delay τ as the TFISH field because of the equal optical path lengths corresponding to the upper and lower arms of the setup. To assure that this is completely fulfilled in experiment, an additional tuning can be introduced by inserting an auxiliary delay line.

The operator for the signal we are interested in is given by the difference of number of photons between the pair of balanced photodetectors, $\hat{N}_2 - \hat{N}_1 \equiv \hat{S}_{\text{hom}}$, with

$$\hat{S}_{\text{hom}} = C' A \int_0^\infty \frac{d\omega_2}{\hbar \omega_2} n(\omega_2) \eta(\omega_2) e^{i\phi} f_{\text{LO}}^*(\omega_2) \hat{E}_{2P}(\omega_2) + \text{H.c.}, \quad (3)$$

where $C' = 4\pi c \epsilon_0 F$, F is the effective detection area and $\eta(\omega)$ is the frequency-dependent quantum efficiency of the photodetectors. Using the decomposition of \hat{E}_{2P} given by Equation (2), we can write \hat{S}_{hom} as $\hat{S}_{\text{hom}} = \hat{S} + \hat{S}_B$, with \hat{S}_B corresponding to the background vacuum signal, and

$$\hat{S}(\tau) = C'' \int_0^\infty d\Omega \mathcal{G}_\phi(\Omega) e^{-i\Omega\tau} \hat{E}_T(\Omega) + \text{H.c.}, \quad (4)$$

where $C'' = 6\pi \epsilon_0 F d\chi^{(3)} \sqrt{\eta_2} R \sqrt{1 - R} A_P^3 / \hbar$ and the resulting gating function, limiting the effective integration range in Equation (4) to THz frequencies, is given by

$$\begin{aligned} \mathcal{G}_\phi(\Omega) &= i e^{i\phi} \mathcal{G}_-(\Omega) - i e^{-i\phi} \mathcal{G}_+(\Omega); \\ \mathcal{G}_\pm(\Omega) &= \int_0^{\omega_{\text{cut}}} d\omega_2 \eta(\omega_2) f_{\text{LO}}^*(\omega_2) (f * f)(\omega_2 \pm \Omega). \end{aligned} \quad (5)$$

We have introduced ω_{cut} to represent an optional upper spectral limit for the collected NIR photons, as discussed below. Deriving Equation (4), we switched the order of integrations between the integral of Equation (3) and that of the convolution coming there from Equation (2). Casting the electric field operator in terms of creation $a_T^\dagger(\Omega)$ and annihilation $a_T(\Omega)$ operators, leading to $\hat{E}_T(\Omega) = -i\sqrt{\hbar\Omega/C'n(\Omega)} \hat{a}_T(\Omega)$ for $\Omega > 0$, the TFISH induced contribution to the homodyne signal can be rearranged as

$$\hat{S}(\tau) = \frac{-iC''}{\sqrt{C'}} \int_0^\infty \frac{d\Omega \sqrt{\hbar\Omega}}{\sqrt{n(\Omega)}} \mathcal{G}_\phi(\Omega) e^{-i\Omega\tau} \hat{a}_T(\Omega) + \text{H.c.} \quad (6)$$

In order to obtain the quantum statistics of the operator $\hat{S}(\tau)$ at each time delay τ from the general Equation (6) or (4) and thus to get access to the time-resolved properties of the quantum field \hat{E}_T , we need to assume a particular form of this field.

The simplest case for the consideration is provided by the bare THz vacuum field. In this case, the mean values of both contributions to \hat{S}_{hom} vanish. Further, since these contributions are determined by creation/annihilation operators stemming from different frequency ranges, they are uncorrelated. Thus, the total variance is given by the sum of the variance of the TFISH part,

$$\langle \hat{S}^2 \rangle_{\text{vac}} \equiv \sigma_T^2 = \langle 0 | \hat{S}^2 | 0 \rangle = \frac{C''^2}{C'} \int_0^\infty \frac{d\Omega \hbar \Omega}{n(\Omega)} |\mathcal{G}_\phi(\Omega)|^2, \quad (7)$$

and of the variance originating from the background vacuum in the range of ω_2 frequencies (here we assume $\omega_{\text{cut}} = \infty$),

$$\langle \hat{S}_B^2 \rangle \equiv \sigma_{\text{SN}}^2 = A^2 C' \int_0^\infty \frac{d\omega_2}{\hbar \omega_2} |f_{\text{LO}}(\omega_2)|^2 \eta^2(\omega_2) n(\omega_2). \quad (8)$$

Both variances are independent of the time delay τ . The TFISH part is determined by the properties of the gating function $\mathcal{G}_\phi(\Omega)$, which follow from the relation between $\mathcal{G}_+(\Omega)$ and $\mathcal{G}_-(\Omega)$ and can be influenced by the phase shift ϕ . When the temporal profiles of the TFISH and SHG signals coincide, we

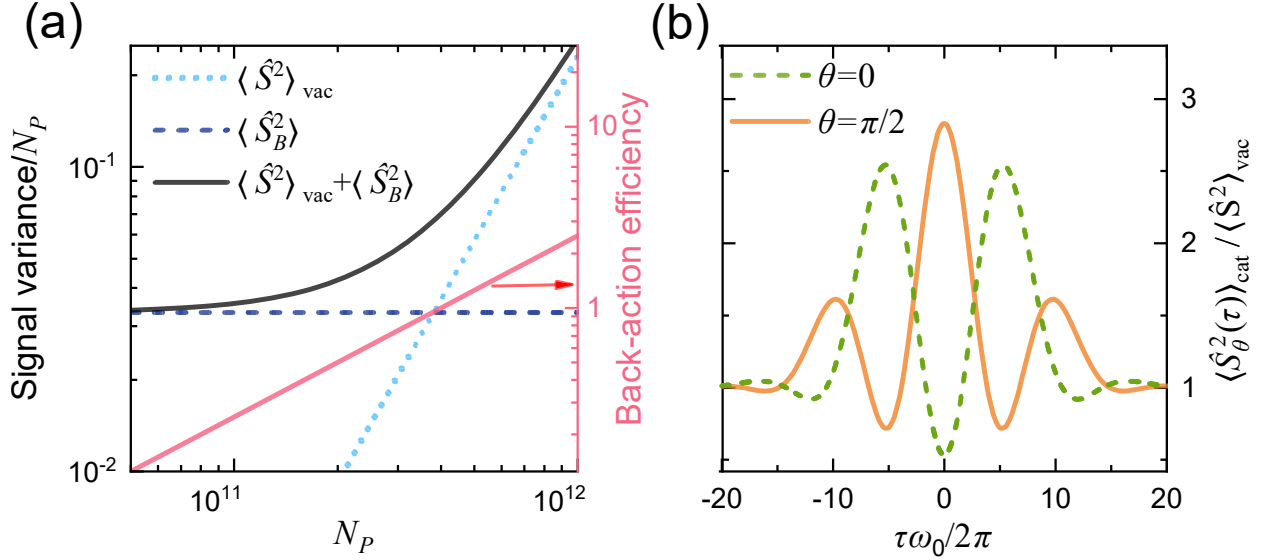


Figure 2: (a) Normalized (by the mean probe photon number N_P) signal variance arising from the THz vacuum $\langle \hat{S}^2 \rangle_{\text{vac}}$ and the background LO vacuum $\langle \hat{S}_B^2 \rangle$ as well as the corresponding (normalized) total variance are shown as functions of N_P , along with a perturbative estimation for the back-action efficiency of the $\chi^{(3)}$ process. Parameter values: $\eta=1$, $\eta_2=0.1$, $R=2/3$, $d = 12 \mu\text{m}$, $\sigma/(2\pi) = 31 \text{ THz}$, $\omega_0/(2\pi) = 193 \text{ THz}$, $\chi^{(3)} = 2.5 \times 10^{-21} \text{ m}^2/\text{V}^2$, $n=2.4$, $F = 9 \mu\text{m}^2$. (b) TFISH signal variance for a broadband cat state, $\langle \hat{S}_\theta^2(\tau) \rangle - \langle \hat{S}_\theta(\tau) \rangle^2 = \langle \hat{S}_\theta^2(\tau) \rangle$, normalized by its bare vacuum counterpart. Both generalized quadratures, corresponding to $\theta = 0$ and $\theta = \pi/2$, respectively, are shown in dependence on the time delay τ . The cat state is composed of a superposition of two broadband coherent states, with opposite amplitudes having Gaussian frequency distributions of central frequency $\Omega_{\text{THz}} = 0.26\omega_0$ and width $\sigma_{\text{THz}} = 0.13\omega_0$, so that the mean photon number is $\langle \text{cat} | \hat{N} | \text{cat} \rangle = 1$. For detection, $\omega_{\text{cut}} = 2\omega_0$ is used.

have $\mathcal{G}_+(\Omega) = \mathcal{G}_-^*(\Omega)$. Then $\mathcal{G}_\phi(\Omega)$ is real and vanishes for $\phi = 0$. Its absolute value is maximized for $\phi = \pm\pi/2$, with $|\mathcal{G}_\phi(\Omega)| = |\mathcal{G}_+(\Omega) + \mathcal{G}_-^*(\Omega)| = 2|\text{Re}(\mathcal{G}_+(\Omega))|$, representing the optimal configuration for the sampling of the THz vacuum. With $\hat{S}_{\text{hom}} = \hat{S}_B$ for $\phi = 0$, the corresponding measurement outcomes can be used for the elimination of the background NIR vacuum contribution on the pulse-by-pulse basis (self-referencing), alternating the CEP by $\pi/2$ between the pulses (see **Figure 1c**).

In order to sample THz quantum fields beyond the bare vacuum, we need to get access to both generalized quadratures of the sampled field in the time domain [28, 24, 25]. This is possible to achieve with a variation of the proposed setup, introducing an asymmetry between $\mathcal{G}_+(\Omega)$ and $\mathcal{G}_-(\Omega)$ contributions to $\mathcal{G}_\phi(\Omega)$. One of the easiest ways to realize this, suitable for our discussion here, is based on the cuts in the spectra of the detected photons that can be implemented via the corresponding frequency band-pass filters [25, 30]. Looking at the second line of Equation (5) one can anticipate that, e.g., for a band-pass filter cutting the frequencies above the central frequency of the LO, $\mathcal{G}_-(\Omega)$ dominates over $\mathcal{G}_+(\Omega)$ in terms of the absolute magnitude and $\mathcal{G}_\phi(\Omega)$ becomes complex. In the easiest case, it can be written as $\mathcal{G}_\phi(\Omega) = |\mathcal{G}_\phi(\Omega)|e^{i\theta}$, where the phase $\theta = \theta(\phi)$ is uniquely determined by the phase ϕ (and vice versa) whereas being independent of frequency. In particular, we have $\theta = \pi/2$ for $\phi = 0$ and $\theta = 0$ for $\phi = -\pi/2$. Then we can introduce operators $\hat{S}_0(\tau)$ and $\hat{S}_{\pi/2}(\tau)$, with $\phi = -\pi/2$ and $\phi = 0$ in Equation (4), respectively. These operators determine both generalized quadratures of the sampled quantum field, up to normalization prefactors. Measuring at $\theta = \pi/2$ ($\phi = 0$), we do not get a direct access to the background NIR vacuum signal $\langle \hat{S}_{B,\text{cut}}^2 \rangle$ for the self-referencing. However, its contribution to the calculated signals is the same for both generalized quadratures. Therefore, measurements for both $\theta = 0$ and $\theta = \pi/2$, with and without the frequency cut, provide sufficient information to calculate $\langle \hat{S}_{B,\text{cut}}^2 \rangle = \langle \hat{S}_B^2 \rangle \langle \hat{S}_{\text{hom,cut}}^2 \rangle / \langle \hat{S}_{\text{hom}}^2 \rangle$ required for the self-referencing, up to generally minor corrections due to a change in the spectral shape of $\mathcal{G}_{\phi=-\pi/2}(\Omega)$ caused by the cut.

4 Results

Let us first illustrate how the proposed scheme for sampling of quantum fields operates in the case when we apply it to the bare THz vacuum, using typical experimental parameters. We assume that the probe is Gaussian, has central frequency ω_0 and spectral width σ . The LO field has central frequency $2\omega_0$ and spectral width $\sqrt{2}\sigma$. Ignoring dispersion and assuming a flat response for the detector crystal, i.e., $n(\omega_2) = n$ and $\eta(\omega_2) = \eta$ as well as no spectral cuts for the detected photons, meaning $\omega_{\text{cut}} = \infty$ in Equation (5), gives $\mathcal{G}_{\pm}(\Omega) = \eta \exp(-\Omega^2/8\sigma^2)/2\sqrt{2\pi}\sigma$. The TFISH contribution to the variance is maximized for $\phi = -\pi/2$, with $\mathcal{G}_{\phi}(\Omega) = 2\mathcal{G}_{+}(\Omega)$ here. We get then

$$\langle \hat{S}^2 \rangle_{\text{vac}} = \frac{9d^2\eta^2\eta_2(1-R)R^2\sigma^3(\chi^{(3)})^2\omega_0^3\hbar^2}{8\pi^{3/2}c^4n^4\epsilon_0^2F^2}N_P^3, \quad (9)$$

where $N_P = A_P^2nC' \int_0^\infty \frac{f^2(\omega)d\omega}{\hbar\omega} \approx \frac{A_P^2nC'}{2\sqrt{\pi}\hbar\sigma\omega_0}$ is the average number of photons in the probe. Under the same conditions, we obtain

$$\langle \hat{S}_B^2 \rangle \approx A^2C' \frac{n\eta^2}{2\sqrt{\pi}\hbar\sigma\omega_0} = \eta^2\eta_2(1-R)N_P. \quad (10)$$

Figure 2a shows $\langle \hat{S}^2 \rangle_{\text{vac}}$, $\langle \hat{S}_B^2 \rangle$ and the total variance $\langle \hat{S}_{\text{hom}}^2 \rangle$ as functions of the number of photons in the probe pulse, contrasted with an estimation of the back-action efficiency of the $\chi^{(3)}$ process in the perturbative regime (see Supporting Information for details). We choose the parameters considering a probe laser with $1.55 \mu\text{m}$ central wavelength and 6 fs pulse duration and a thin $12 \mu\text{m}$ slab of diamond for the $\chi^{(3)}$ crystal. The variance of the TFISH part surpasses the variance due to the background vacuum at around $N_P = 3.7 \times 10^{11}$ photons per pulse. However, the back-action becomes significant around the same photon number, thus invalidating the perturbative approach. To prevent this, N_P can be chosen at a lower value, implementing a weak measurement. To achieve the required signal-to-noise ratio, the measurement results can be then averaged over a sufficient number of probe pulses, as in [20, 27, 22]. As an illustration of the scheme going beyond sampling of the THz quantum vacuum, **Figure 2b** shows the variance signals for a broadband cat state, as a function of the time delay of the probe. The utilized cat state is defined as $|\text{cat}\rangle \propto |\{\alpha_\Omega\}\rangle + |{-\alpha_\Omega}\rangle$, where $|\{\alpha_\Omega\}\rangle$ represents a continuous multimode coherent state with the spectral amplitudes α_Ω corresponding to a classical few-cycle THz pulse [38, p. 85]. To access both quadratures, we performed the frequency cut on the spectral content of the photons collected by the photodetectors, determining the gating function, Equation (5), by choosing $\omega_{\text{cut}} = 2\omega_0$. Further details on the calculation are given in Supporting Information.

5 Conclusion

We have developed a new scheme for sampling of quantum fields in the time domain and illustrated it by calculating the electric-field variance and its dynamics for the quantum vacuum and a pulsed broadband cat state, respectively. The scheme is feasible for typical experimental parameters and has a number of intrinsic advantages, such as automatic subtraction of the contaminating shot-noise by the shot-by-shot self-referencing. High sensitivity in the 5-15 THz provides the ability to study low-energy quantum dynamics in condensed matter, while frequency filtering of homodyne signal gives access to both generalized electric-field quadratures, en route toward subcycle quantum tomography. Finally, lifting the reliance on high-precision polarization optics holds promise for future imaging and microscopy applications involving THz and MIR quantum fields.

Supporting Information

Supporting Information is available from the Wiley Online Library or from the author.

Acknowledgements

This research was supported by the National Research Foundation of Korea (NRF) grant funded by the Korea government (MSIT)(2020R1A2C1008500). A.S.M was also supported by the Mercator Fellow-

ship of the Deutsche Forschungsgemeinschaft (DFG) - Project No. 425217212 - SFB 1432 and Baden-Württemberg Stiftung via the Elite Programme for Postdocs. S.G. acknowledges support by the Institute for Basic Science in Korea (IBS-R024-D1). S.V., M.S. and D.V.S. acknowledge funding by the Natural Sciences and Engineering Research Council of Canada (NSERC) via the Canada Research Chair (CRC) of D.V.S. and the Fonds de Recherche du Québec –Nature et Technologies (FRQNT) via Institut Transdisciplinaire d’Information Quantique (INTRIQ). Further, this project has received funding from the European Union’s Horizon Europe research and innovation programme under grant agreement No. 101070700.

References

- [1] M. Collett, R. Loudon, C. Gardiner, *J. Mod. Opt.* **1987**, *34* 881.
- [2] A. I. Lvovsky, M. G. Raymer, *Rev. Mod. Phys.* **2009**, *81* 299.
- [3] A. Schliesser, N. Picqué, T. Hänsch, *Nat. Photon.* **2012**, *6* 440.
- [4] F. Krausz, M. Ivanov, *Rev. Mod. Phys.* **2009**, *81* 163.
- [5] Q. Wu, X. Zhang, *Appl. Phys. Lett.* **1995**, *67* 3523.
- [6] G. Gallot, D. Grischkowsky, *J. Opt. Soc. Am. B* **1999**, *16*, 8 1204.
- [7] A. Leitenstorfer, S. Hunsche, J. Shah, M. C. Nuss, W. H. Knox, *Appl. Phys. Lett.* **1999**, *74* 1516.
- [8] Q. Wu, X.-C. Zhang, *Appl. Phys. Lett.* **1997**, *71* 1285.
- [9] C. Kübler, R. Huber, S. Tübel, A. Leitenstorfer, *Appl. Phys. Lett.* **2004**, *85* 3360.
- [10] P. Gaal, M. B. Raschke, K. Reimann, M. Woerner, *Nat. Photon.* **2007**, *1* 577.
- [11] A. Sell, R. Scheu, A. Leitenstorfer, R. Huber, *Appl. Phys. Lett.* **2008**, *93* 251107.
- [12] S. Keiber, S. Sederberg, A. Schwarz, M. Trubetskov, V. Pervak, F. Krausz, N. Karpowicz, *Nat. Photon.* **2016**, *10* 159.
- [13] C. Riek, D. V. Seletskiy, A. Leitenstorfer, *Eur. J. Phys.* **2017**, *38* 024003.
- [14] A. Zavatta, S. Viciani, M. Bellini, *Science* **2004**, *306* 660.
- [15] H. Hansen, T. Aichele, C. Hettich, P. Lodahl, A. I. Lvovsky, J. Mlynek, S. Schiller, *Opt. Lett.* **2001**, *26* 1714.
- [16] A. Eckstein, B. Brecht, C. Silberhorn, *Opt. Express* **2011**, *19* 13770.
- [17] M. E. Anderson, D. F. McAlister, M. G. Raymer, M. C. Gupta, *J. Opt. Soc. Am. B* **1997**, *14* 3180.
- [18] W. Wasilewski, A. I. Lvovsky, K. Banaszek, C. Radzewicz, *Phys. Rev. A* **2006**, *73* 063819.
- [19] M. G. Raymer, I. A. Walmsley, *Phys. Scr.* **2020**, *95* 064002.
- [20] C. Riek, D. V. Seletskiy, A. S. Moskalenko, J. F. Schmidt, P. Krauspe, S. Eckart, S. Eggert, G. Burkard, A. Leitenstorfer, *Science* **2015**, *350*, 6259 420.
- [21] A. S. Moskalenko, C. Riek, D. V. Seletskiy, G. Burkard, A. Leitenstorfer, *Phys. Rev. Lett.* **2015**, *115* 263601.
- [22] I.-C. Benea-Chelms, F. F. Settembrini, G. Scalari, J. Faist, *Nature* **2019**, *568* 202.
- [23] F. F. Settembrini, F. Lindel, A. M. Herter, S. Y. Buhmann, J. Faist, *Nat. Comm.* **2022**, *13* 3383.

- [24] S. Virally, B. Reulet, *Phys. Rev. A* **2019**, *100* 023833.
- [25] P. Sulzer, K. Oguchi, J. Huster, M. Kizmann, T. L. M. Guedes, A. Liehl, C. Beckh, A. S. Moskalenko, G. Burkard, D. V. Seletskiy, A. Leitenstorfer, *Phys. Rev. A* **2020**, *101* 033821.
- [26] S. Virally, P. Cusson, D. V. Seletskiy, *Phys. Rev. Lett.* **2021**, *127* 270504.
- [27] C. Riek, P. Sulzer, M. Seeger, A. S. Moskalenko, G. Burkard, D. V. Seletskiy, A. Leitenstorfer, *Nature* **2017**, *541* 376.
- [28] M. Kizmann, T. L. M. Guedes, D. V. Seletskiy, A. S. Moskalenko, A. Leitenstorfer, G. Burkard, *Nat. Phys.* **2019**, *15*, 9 960.
- [29] F. Lindel, R. Bennett, S. Y. Buhmann, *Phys. Rev. A* **2020**, *102* 041701.
- [30] M. Kizmann, A. S. Moskalenko, A. Leitenstorfer, G. Burkard, S. Mukamel, *Laser Photon. Rev.* **2022**, *16* 2100423.
- [31] C.-Y. Li, D. V. Seletskiy, Z. Yang, M. Sheik-Bahae, *Opt. Express* **2015**, *23* 11436.
- [32] N. Karpowicz, J. Dai, X. Lu, Y. Chen, M. Yamaguchi, H. Zhao, X.-C. Zhang, *Appl. Phys. Lett.* **2008**, *92* 011131.
- [33] A. Tomasino, R. Piccoli, Y. Jestin, B. L. Drogoff, M. Chaker, A. Yurtsever, A. Busacca, L. Razzari, R. Morandotti, *Nanomaterials* **2021**, *11* 283.
- [34] D. Fehrenbacher, P. Sulzer, A. Liehl, T. Kälberer, C. Riek, D. V. Seletskiy, A. Leitenstorfer, *Optica* **2015**, *2* 917.
- [35] R. J. Glauber, *Phys. Rev.* **1963**, *130* 2529.
- [36] T. L. M. Guedes, I. Vakulchyk, D. V. Seletskiy, A. Leitenstorfer, A. S. Moskalenko, G. Burkard, Back action in quantum electro-optic sampling of electromagnetic vacuum fluctuations, *Phys. Rev. Research* **2023**, accepted; arXiv:2202.03353.
- [37] I. Coddington, N. Newbury, W. Swann, *Optica* **2016**, *3* 414.
- [38] W. Vogel, D. Welsch, *Quantum Optics*, Wiley, Weinheim, 3rd edition, **2006**.